Modulation of magnetospheric substorm frequency: Dipole tilt and IMF B_y effects

A. Ohma[1], J. P. Reistad[1], S. M. Hatch[1]

[1]Birkeland Centre for Space Science, University of Bergen, Bergen, Norway

Key Points:

- Substorms are more frequent when the dipole tilt angle and IMF B_y have opposite compared to equal sign
- This is a magnetospheric response, and cannot be explained by magnetosphere-ionosphere coupling affecting detection of substorms at ground
- Whether the combination of B_y and tilt angle affects the dayside reconnection rate or magnetotail processes is currently unresolved

Compiled on 2020/07/27 at 22:09:16

Corresponding author: A. Ohma, `anders.ohma@uib.no`

Abstract

Using five independent substorm onset lists, we show that substorms occur more frequently when the Interplanetary Magnetic Field (IMF) B_y component and the dipole tilt angle Ψ have different signs as opposed to when they have the same sign. These results confirm that the magnetosphere exhibits an explicit B_y effect for $\Psi \neq 0$, as other recent studies have suggested, and imply variation in the dayside reconnection rate and/or the magnetotail response. We additionally observe more frequent onsets for positive B_y in an onset list based on identifying negative bays in the auroral electrojet, regardless of season. Taking into account all five onset lists, we conclude that this phenomenon is not real, but is rather a consequence of the particular substorm identification method, which is affected by local ionospheric conditions that depend on B_y and Ψ.

Plain Language Summary

The solar wind that the Sun continuously emits is a plasma with an embedded magnetic field. The direction in which this magnetic field points changes frequently, and is among the most important factors in controlling geomagnetic activity, or how frequent and how bright the aurorae are. From the perspective of an observer at the magnetic pole in the Northern Hemisphere, a downward-pointing magnetic field yields the highest amount of geomagnetic activity and results in frequent and bright auroral displays. The magnetic field can also have a "sideways" component that points either toward dawn or toward dusk. It is often assumed that geomagnetic activity does not depend on whether the magnetic field points toward dawn or dusk. In this study, we show that around each solstice this sideways component does matter. When Earth is tilted towards the Sun (northern summer/southern winter), a dawnward-pointing magnetic field gives more frequent auroral breakups than the other. When Earth is tilted away from the Sun, a duskward-pointing magnetic field yields more auroral breakups. This insight improves our understanding of how Earth is coupled to space.

1 Introduction

It has recently been documented that certain aspects of the solar wind-magnetosphere-ionosphere coupling exhibit so-called explicit Interplanetary Magnetic Field (IMF) B_y effects. Although first pointed out by Friis-Christensen and Wilhjelm (1975), Holappa and Mursula (2018) further demonstrated and quantified the influence on the westward electrojet by the sign of IMF B_y (hereafter B_y). They found that during local winter in the northern hemisphere, the AL index was $\sim$50% greater for positive B_y compared to negative B_y, during otherwise similar conditions. Similar differences have also been reported in Birkeland currents derived from the Average Magnetic field and Polar current Systems (AMPS) model (Laundal et al., 2018).

In lieu of a satisfying explanation of the dependence of ionospheric currents on the polarity of B_y, further studies have revealed other aspects of the coupled solar wind-magnetosphere-ionosphere system that exhibit similar dependence on B_y polarity. Reistad et al. (2020) found that the average size of the Region 1/Region 2 (R1/R2) current system, approximated as the radius of a circle fitted to Active Magnetospheric and Planetary Electrodynamics Response Experiment (AMPERE) observations, was significantly different under positive and negative B_y. This difference was only evident when the Earth's dipole tilt angle Ψ (i.e., degree of tilt of the Earth's dipole axis along the Sun-Earth line) was large. By convention, $\Psi < 0$ corresponds to December solstice (northern winter/southern summer). Specifically, they found that for large, negative Ψ, positive B_y results on average in a slightly larger radius than negative B_y during otherwise similar conditions, as parameterized by a solar wind-magnetosphere coupling function (Milan et al., 2012). On the other hand, for large, positive Ψ (i.e., near June solstice) the radius of the R1/R2 current system has an opposite dependence on the sign of B_y. The same results were obtained from independent data in both hemispheres, which strongly suggests that this in not an effect of different magnetosphere-ionosphere (M-I) coupling in the two hemispheres, but is rather an effect of solar wind-magnetosphere interactions.

Holappa et al. (2020) recently reported a similar B_y polarity effect in the fluxes of high energy electron precipitation (> 30 keV) in the auroral region, most notably in the midnight to morning local time sector. They found significantly larger fluxes during the same conditions for which Reistad et al. (2020) find a larger radius of the R1/R2 current system. Furthermore, their results are consistently seen in both hemispheres. Again, this strongly suggests that the cause of their observed asymmetry is not an effect of the different M-I coupling in the two hemispheres, but rather linked to a property of the solar wind-magnetosphere interactions.

Liou et al. (2020) investigated substorm occurrence rates with special emphasis on the sign of B_y, also taking into account the level of upstream forcing. Their analysis indicated a trend of ∼30% more substorms during positive compared to negative B_y. However, Liou et al. (2020) only considered substorm lists based on detecting negative bays in the *SML* index (Newell & Gjerloev, 2011a), and did not sort their analysis with respect to dipole tilt or any other seasonal parameter. Here we demonstrate that both the underlying substorm signature used to identify onsets and seasonal parameters may influence the conclusions drawn from the analysis of substorm occurrence rates.

This paper presents analysis of five independent lists of substorm onsets, all of which are sorted by IMF clock angle and dipole tilt angle. These lists and our methodology for processing them are described in the following section. We show the resulting onset frequency distributions in section 3. We discuss the significance and physical implications of the results in section 4, and summarize our findings in section 5.

2 Data processing

To determine how the substorm frequency depends on B_y and Ψ, we employ five substorm onset lists, each based on different onset signatures from independent data sets. Multiple lists are used to ensure that the observed trends are a signature of the magnetospheric response, and not the result of M-I coupling or the local conditions in the hemisphere where the observations are taken. The five substorm onset lists utilized in this study are introduced below.

1. A distinct aspect of substorms is a negative bay in ground magnetometers at auroral latitudes, caused by an enhancement of the westward electrojet as the substorm current wedge closes in the ionosphere. The *SML* index (Newell & Gjerloev, 2011a) quantifies the strength of the westward electrojet, and is based on ∼100 magnetometer stations at auroral latitudes in the northern hemisphere from the SuperMAG network of ground observatories (Gjerloev, 2012). Using an algorithm to identify sharp and sustained drops in the *SML* index, Newell and Gjerloev (2011a, 2011b), present an onset list (hereafter the N&G list) that consists of 70,278 onsets identified during 1981–2019.
2. Positive bays in magnetometer data at mid-latitudes are a signature of field-aligned currents associated with the substorm current wedge. A mid-latitude positive bay (MPB) index using 41 ground magnetometers in both hemispheres was put forward by Chu et al. (2015); this index can be used to identify substorm onset by identifying bay signatures (Chu et al., 2015; McPherron & Chu, 2018). We have used the onset list described in McPherron and Chu (2018) (hereafter the McP&C list), which consists of 57,558 onsets in the years 1982–2012 when their proposed threshold value of the area of the positive bays, > 700 nT^2-min, is used.
3. Another signature of substorm onset is Pi2 pulsations, which are oscillations in the geomagnetic field observed at low- and mid-latitudes. A related index, termed

the Wave and planetary (Wp) index, was proposed by Nosé et al. (2012). This index is based on 1-s magnetometer observations from 11 stations at low- and mid-latitudes, and is believed to reflect the wave power of the Pi2 pulsations. Nosé et al. (2012) also proposed threshold criteria for identifying substorm onsets from the Wp index. Using these criteria, we identify 14,075 onsets during 2005–2019 (hereafter the Nosé list).

4. Substorms are associated with a sudden, localized brightening of the aurora, which expands both longitudinally and poleward as the substorm progresses (Akasofu, 1964). We have used a combination of two onset lists based on global far-ultraviolet images of the aurora made by the IMAGE mission (Frey et al., 2004; Frey & Mende, 2006) and the Polar mission (Liou, 2010). These lists yield a combined total of 6,727 identified substorm onsets during 1996–2007. We refer to this combined list as the F+L list. Note that each list is based on images from a single orbiting spacecraft, which means that each spacecraft can only detect a substorm when it occurs within the field of view of the imaging instrument. Hence, this list does not provide full coverage of the given years. About 1/3 of the IMAGE onsets and about 1/5 of the Polar onsets are from the southern hemisphere.
5. Yet another signature of substorm onset is the injection of energetic electrons into geosynchronous orbit (Kamide & McIlwain, 1974; Yeoman et al., 1994; Weygand et al., 2008), which leads to a sharp drop in the specific entropy of the hot electron population (e.g. Borovsky & Cayton, 2011). Borovsky and Yakymenko (2017) present a substorm onset list (hereafter the B&Y list) based on identification of such drops using the Synchronous Orbit Particle Analyzer (SOPA) instrument on various geosynchronous spacecraft. The B&Y list is available at 30-min resolution, and gives 16,025 onsets in the years 1989–2007. Since the electron injection must drift to an orbiting spacecraft in order to be detected, the onsets determined by this method are systematically delayed by 0–30 min compared to the other lists. To account for this statistical bias, we have shifted the onsets in this list by -15 min.

Before comparing substorm occurrence rates, we identify a potential source of bias in this analysis and describe how we account for it. Figure 1 displays the distribution of the clock angle θ_{CA} during 1981–2019 in Geocentric Solar Magnetic (GSM) coordinates, Geocentric Solar Ecliptic (GSE) coordinates and Geocentric Solar Equatorial (GSEq) coordinates for $\Psi < -15^\circ$ and $\Psi > 15^\circ$ using a bin size of 5°. These θ_{CA} values were calculated from the OMNI 1-min data, which is propagated to the nose of the Earth's bow shock (King & Papitashvili, 2005). Rotation of the IMF vectors to GSEq coordinates were done with the aid of the International Radiation Belt Environment Modeling (IRBEM) library (Boscher et al., 2004–2008) using SpacePy 0.2.1 (Morley et al., 2011).

While the two distributions are similar in GSEq coordinates, they are not similar in GSE and GSM coordinates; rather, they are rotated in opposite directions relative to the distributions in GSEq coordinates. For negative B_y, this apparent rotation corresponds to more southward and less northward IMF for positive tilt angles compared to negative tilt angles, and vice versa for positive B_y. This is the well known Russell-McPherron effect (Russell & McPherron, 1973), which describes how mapping from GSEq coordinates to GSM coordinates leads to seasonal biases in the clock angle distribution, and hence different levels of geomagnetic activity depending on the sign of the B_y component. The effect maximizes around equinoxes, but is also substantial near solstices. While the effect near equinoxes is due to the large angle between Earth's rotational axis and the normal of the ecliptic, the effect near solstice is due to the angle between the ecliptic and the Sun's equatorial plane.

We account for these season-related biases in the IMF orientation as follows. We bin the onsets by the average IMF clock angle in the hour before each onset, and use the deciles of the absolute clock angle distribution during 1981–2019 to determine the bin size; this yields 10 bins containing approximately the same number of hours of data. We

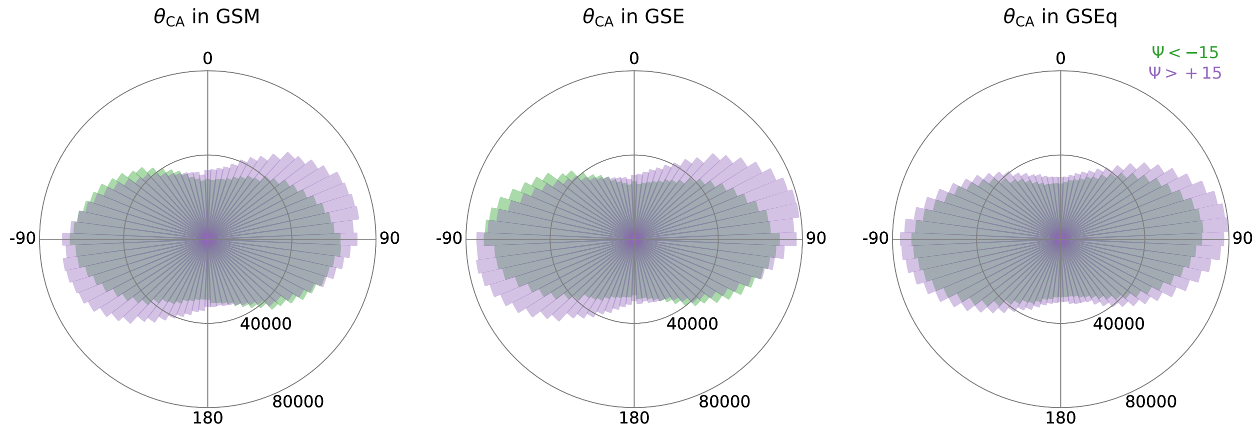

Figure 1. IMF clock angle distribution for $\Psi < -15°$ (green) and $\Psi > 15°$ (purple) in GSM (left), GSE (middle) and GSEq (right) coordinates.

then normalize each clock angle bin by the number of days that the IMF clock angle has that particular range of orientations over the duration of each specific substorm list; thus each bin has units of frequency of substorm onsets per day. Last, we divide the data into groups based on dipole tilt angle, Ψ, which was calculated using the method described in Laundal and Richmond (2017).

3 Results

The distributions of substorm onsets per day are given in Figure 2. Each row corresponds to an independent substorm list, and each column corresponds to a different tilt angle interval. Blue and orange indicate negative and positive B_y, respectively. The numbers in the upper left corner of each panel are the total number of substorms for $\pm B_y$ identified by the onset identification method associate with that list, and the ratio of positive B_y to negative B_y onsets (black). The numbers in the lower right corner are the average number of substorms per day found by averaging the distributions in each panel, and the ratio of positive B_y to negative B_y onsets per day. These latter numbers are based on the binned data, in which biases in the clock angle distribution are accounted for.

From the figure, it is immediately clear that the distributions for positive and negative B_y are different for large tilt angles. For $\Psi < -15°$, there are more onsets per day for positive B_y than for negative B_y. This in most clear in the N&G list (top row), but consistently seen in all onset lists. The opposite effect is seen when $\Psi > 15°$, where there are more onsets per day for negative than positive B_y, again seen in all the list, albeit less pronounced in the N&G and McP&C lists. The effect is most notable for $45° < |\theta_{CA}| < 135°$, which is when B_y dominates. That most of the asymmetry in onset frequency remains after binning by clock angle (lower right in each panel), strongly suggests that non-zero dipole tilt modulates the substorm frequency, in addition to any asymmetry caused by the different clock angle distribution.

In the $|\Psi| < 15°$ tilt interval (second column) the distributions for $\pm B_y$ are similar and the average number of onsets per day about the same, with the notable exception of the N&G list, in which there are considerably more onsets for $B_y > 0$. In the rightmost column of the figure we show the two distributions that result when no restriction is place on Ψ. These distributions are very similar to the $|\Psi| < 15°$ distributions, with very similar distributions for $\pm B_y$ for all lists except the N&G list.

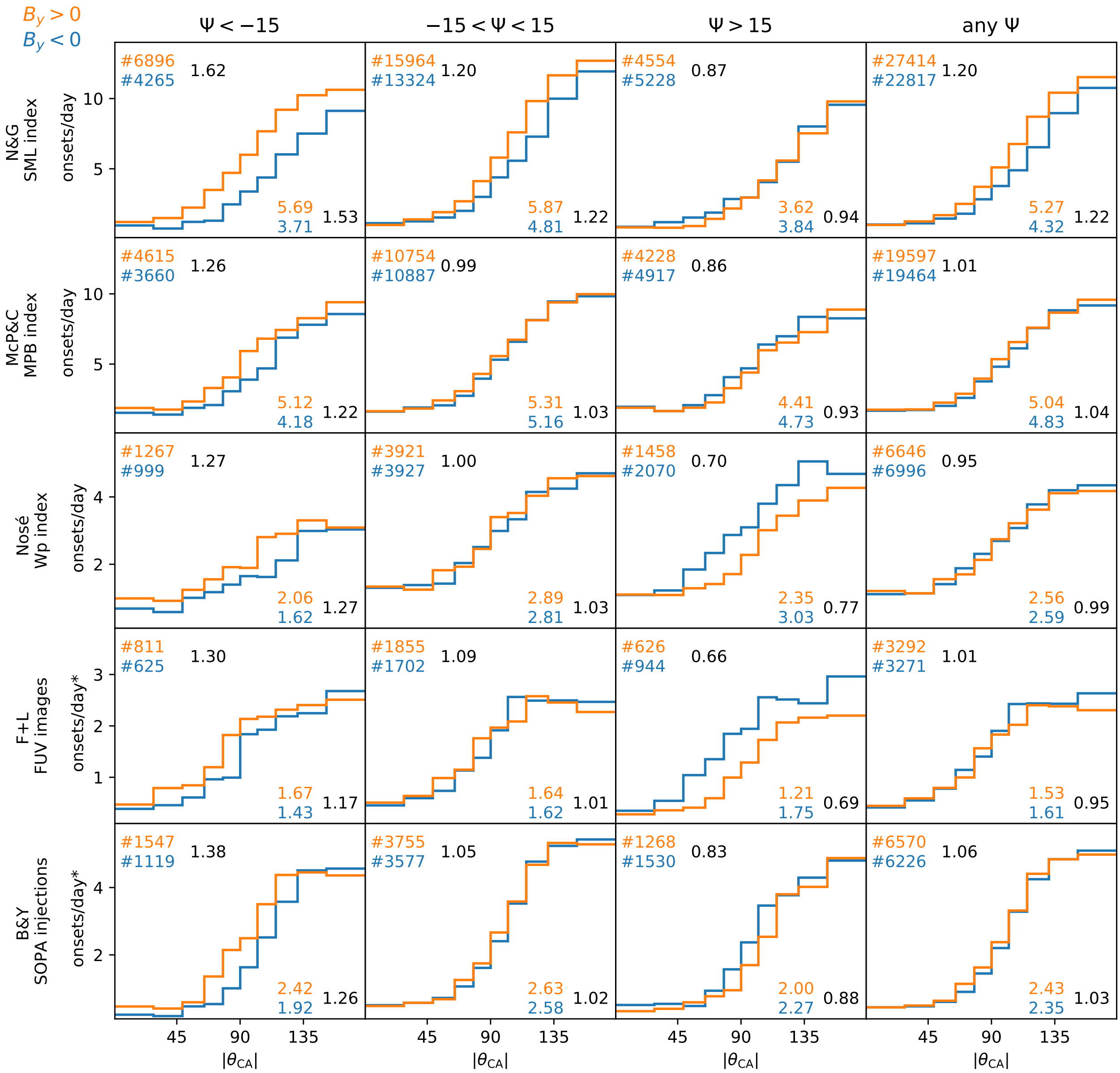

Figure 2. Onset occurrence rate for the five independent substorm onset lists. Blue colors indicate IMF $B_y < 0$ and orange colors indicate IMF $B_y > 0$. The numbers in the upper left corner of each panel are the number of onsets for $\pm B_y$, and the fraction of positive to negative onsets. The numbers in the lower right corner of each panel are the average number of substorms per day for $\pm B_y$, and the fraction of positive to negative onsets per day. The '*' symbol indicates lists based on spaceborne instruments, which do not have continuous coverage.

Potential biases in the solar wind forcing could influence the distributions in Figure 2, although a large portion of any such bias is already accounted for by binning on clock angle. Regardless, we have checked this by calculating the bin averages of the mean solar wind forcing in the hour before onset using the Milan et al. (2012) solar wind coupling function (Figure S1 in the Supporting Information). We find no systematic biases that can explain the differences in the onset distributions. The mean solar wind forcing is typically a few percent larger for positive B_y, but this bias is consistent in all tilt angle intervals.

Newell et al. (2016) reported that the solar wind speed is the best predictor of substorm probability. To check for potential biases, we repeat the above using only the solar wind speed (Figure S2 in the Supporting Information). Again, we observe no underlying biases that could explain the onset distributions. A bias towards higher speeds for $B_y > 0$ is seen in the B&Y list, which might explain the slightly higher onset frequency for positive B_y seen in this list.

4 Discussion

Despite being derived from independent data sources, the analysis of each of the five substorm lists shown in Figure 2 shows the same general trend: More frequent substorms when the sign of B_y and Ψ are opposite. However, there are important differences among the lists that we now discuss in more detail.

As the nature of a substorm is magnetospheric, and hence global, a defining signature of a substorm should ideally depend neither on season, nor on the hemisphere from which the observation is made, nor on the spatial coverage of the observing network used. One type of substorm list that is particularly sensitive to the local ionospheric conditions and also M-I coupling effects in general, are substorm lists based on auroral electrojet indices. The upsides of these lists are good observational coverage in the northern hemisphere auroral region and sensitivity to magnetospheric activations. However, the magnetic response at ground level is very much influenced by the ionospheric conductivity and the large-scale geometry of the high-latitude electrodynamics; these are generally different in the two hemispheres. Since the geometry of the polar electrodynamics changes vastly for $\pm B_y$ and dipole tilt angle, investigating how magnetospheric substorm occurrence rates vary with these conditions can be highly problematic.

In our analysis we have included one such list (N&G), but the same trend seen in this list is also is seen in other onset lists based on the *SML* index (Forsyth et al., 2015; Borovsky & Yakymenko, 2017, not shown). We argue that the trend seen for small dipole tilt and for no restriction on dipole tilt (second and rightmost columns, respectively, in Figure 2)—namely that there is a general preference for more frequent substorms when B_y is positive—is not real. This is most likely an artifact of how the auroral electrodynamics are established differently for $\pm B_y$, and not directly related to the processes in the tail initiating nightside activity.

To highlight this point, Figure 3 displays a superposed epoch analysis of the AL index, centered at substorm onsets identified by McP&C. This analysis includes only substorm onsets for which the average clock angle in the hour before onset are in the interval $45° < |\theta_{\mathrm{CA}}| < 135°$. Each column corresponds to a different dipole tilt interval. To mitigate the challenges highlighted by Figure 1, the analysis is further split into three different intervals of average solar wind forcing Φ_D in the hour before onset, using the coupling function reported by Milan et al. (2012). Blue and orange indicate negative and positive B_y, respectively, and the shaded area indicates the standard error of the mean. The numbers in the lower right corner indicate the drop for each curve. This value was determined by subtracting the minimum values from the maximum value near onset (±5 min).

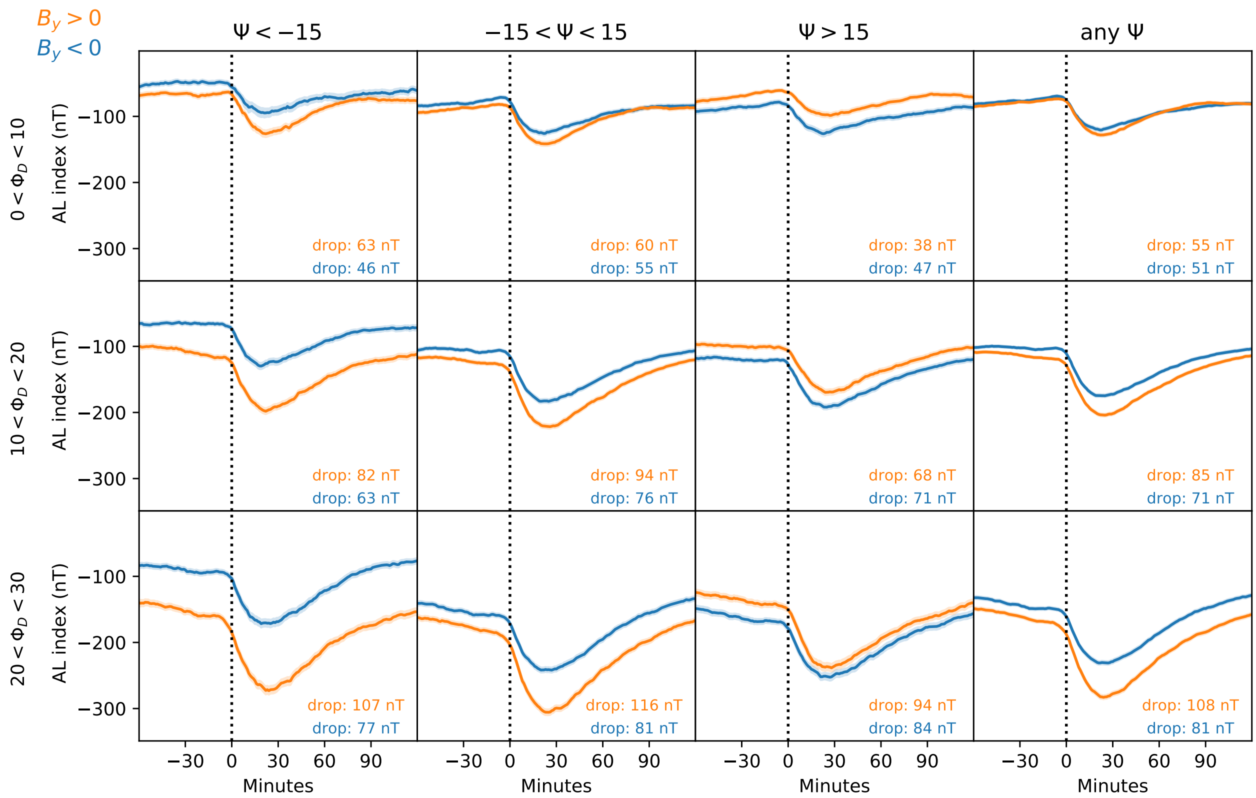

Figure 3. Superposed epoch analysis of the AL index relative to substorm onset in the McP&C list, for different levels of solar wind forcing and tilt angle intervals. Zero epoch corresponds to substorm onset. Blue and orange indicate negative and positive B_y, respectively. Only onsets for which the average clock angle in the hour before onset θ_{CA} are in the interval $45° < |\theta_{\mathrm{CA}}| < 135°$ are included.

From Figure 3, we observe an opposite trend for $\pm B_y$ when Ψ is large; the average curve for positive B_y is below the average curve for negative B_y when $\Psi < -15°$, and vice versa for $\Psi > 15°$. The trend is significantly more pronounced for $\Psi < -15°$. These observations are in agreement with the monthly averages of the AL index presented by Holappa and Mursula (2018). For $|\Psi| < 15°$ and for any Ψ (second and rightmost columns) the curves for $\pm B_y$ are similar for $\Phi_D < 10$ kV (top row), but the curve for $B_y > 0$ is below the curve for $B_y < 0$ for stronger solar wind forcing (middle and bottom rows). We also note that the negative bays are more pronounced for $B_y > 0$, with a sharper and deeper drop, in nearly all subsets. This illustrates how any algorithm designed to identify sharp and/or sustained drops in auroral electrojet–based indices is more prone to detect onsets when $B_y > 0$ compared to $B_y < 0$.

There also appears to be a seasonal bias in the Nosé list, as the total number of substorms are significantly lower for $\Psi < -15°$ compared to $\Psi > 15°$ (middle row in Figure 2. Such bias is not apparent in any of the other lists, which instead indicate that the total number of onsets is about equal for large tilt angles. This bias could be a result of the local season in which the observations are obtained, as only 3 of 11 observatories are located in the southern hemisphere. However, the general trend for $\pm B_y$ in the list is in agreement with the observations from the other lists.

The remaining three substorm lists shown in Figure 2 are less affected by the local hemisphere ionospheric conditions, as their respective onset identification criteria target the global signature of the substorm to larger degrees. These three lists all agree, with little to no difference in onset frequency for the two B_y polarities, during small dipole tilt conditions. Hence, in contrast to (Liou et al., 2020), we conclude that there is no strong general trend toward more substorms when B_y is positive compared to negative, regardless of the dipole tilt orientation. The analysis we have presented reveals to the contrary that the orientation of the dipole axis, together with the orientation of B_y, plays an important role in modulating the substorm onset frequency, which to our knowledge has not been shown earlier. The results in Figure 2 seem to complement those of Holappa et al. (2020), who found larger fluxes of high-energy electron precipitation in both hemispheres for opposite compared to equal sign of B_y and Ψ. The increased substorm frequency for opposite sign of the two parameters could explain the larger fluxes of high-energy electrons observed in the ionosphere, as high-energy precipitation is known to be sensitive to inner magnetospheric activations such as substorms (Beharrell et al., 2015).

The higher occurrence frequency of substorms for opposite compared to equal signs of B_y and Ψ can be interpreted in two ways: 1) Dayside opening of magnetic flux depends on the combination of B_y and Ψ; 2) The magnetotail responds differently to the same loading of magnetic flux for the different combinations of B_y and Ψ. We elaborate briefly on these two scenarios.

The shocked solar wind plasma, which interacts with the dayside magnetopause, has different properties in the pre-noon and post-noon sectors due to the prevailing Parker spiral structure of the IMF. As shown by, e.g., Walsh et al. (2014), the plasma β is typically larger in the pre-noon magnetosheath plasma. These dawn-dusk asymmetries in the shocked solar wind plasma may affect the conditions for reconnection, which is thought to be more effective in low-β regions (Paschmann et al., 1986; Koga et al., 2019). The quasi-parallel shock region (dawn) is also more prone than the quasi-perpendicular region (dusk) to the development of Kelvin-Helmholtz-Instabilities (KHI) (Dimmock et al., 2016; Nykyri et al., 2017). This leads to a dawn-favored plasma entry into the magnetosphere through reconnection inside the KHI vortices.

However, a dawn-dusk asymmetry is alone insufficient to explain putative B_y polarity effects on dayside reconnection, since the reconnection geometry for positive and negative B_y is symmetric if $\Psi = 0°$, only mirrored across the Y_{GSM} axis. Therefore, although the reconnection rates might be different between the pre-noon and post-noon sectors, the rates within each sector remain the same for both polarities of B_y when $\Psi = 0$. Thus the total rate of flux opening is the same regardless of the polarity of B_y. This is consistent with the four onset lists showing little or no B_y polarity effect for small Ψ. This situation changes when Ψ is large. Under these conditions the two hemispheres are not symmetrically exposed to the solar wind and IMF, and differences can arise.

It is unfortunately not possible at present to relate substorm strength and frequency to changes in dayside reconnection rate. Not only is the fraction of flux closure through substorms to the opening of flux on the dayside unknown, it may also depend on Ψ and B_y. Quantitative estimates of the degree of influence on the total dayside reconnection rate, including all the relevant physics, remain a theoretical and observational challenge.

An alternative explanation is that the tail responds differently for opposite and equal signs of B_y and Ψ. If we assume that the dayside reconnection rate is unaffected by B_y polarity, the same amount of flux is added to the magnetosphere for $\pm B_y$. This means that the same amount of flux must, at some point, close again in the tail. Since the observed substorm frequency does vary with B_y polarity and dipole tilt, this could either mean that the average amount of flux closed by the substorms also differs (e.g., more frequent and weaker substorms for B_y and Ψ with opposite signs, and less frequent and stronger substorms for B_y and Ψ with the same sign), that substorms are more prone to lead to steady magnetospheric convection (SMC) (c.f. Sergeev et al., 1996) for one combination that the other, or that the flux throughput is accommodated without initiating substorms.

It may be relevant to look at the relative change of the average negative bays to quantify the strength of the superposed substorm. Based on the numbers in Figure 3, the drop in the AL index is larger for both polarities of B_y when the sign of Ψ is opposite compared to when the sign of Ψ is the same. This indicates that the substorms are not only more frequent, but also stronger, when B_y and Ψ have opposite signs. However, we emphasise that these numbers could be highly influenced by the local ionospheric conditions, and therefore not reflect the amount of flux closed by tail reconnection.

While we do not conjecture why the tail should respond differently, it is in any case known that the geometry of the closed tail is influenced both by Ψ and B_y. It is possible that a combination of plasma sheet warping for $\Psi \neq 0$ (Russell & Brody, 1967; Fairfield, 1980; Tsyganenko & Fairfield, 2004) and plasma sheet rotation when $B_y \neq 0$ (Cowley, 1981; Liou & Newell, 2010) causes different conditions for tail reconnection and substorm activation in the pre-midnight sector, where substorms are preferably initiated (Frey et al., 2004; Liou, 2010; Grocott et al., 2010). It has also been shown by Milan et al. (2019) that high-latitude onsets are more prone to develop into SMC events, whereas low-latitude onsets experience convection-breaking (Grocott et al., 2009) that leads to loading-unloading cycles. Furthermore, the average size of the polar cap is expanded for opposite compared to equal sign of B_y and Ψ (Reistad et al., 2020); this effect might also influence the substorm occurrence rates.

5 Summary

Using five independent substorm onset lists, we have shown that the substorm frequency depends on the sign of IMF B_y when the Earth's dipole tilt angle is large. Specifically, we find a higher substorm frequency when B_y and Ψ have opposite compared to equal signs. Since substorms are a global, magnetospheric process, this confirms that substorm-related magnetospheric processes explicitly depend on the polarity of B_y. We have outlined possible physical mechanisms, and pointed out the present lack of a coherent understanding of these processes. This should encourage further research effort into determining why some magnetospheric processes depend explicitly on the sign of B_y.

With the exception of one onset list that is based on identifying negative bays in the westward electrojet, we find little or no difference in the substorm frequency for $\pm B_y$ for small tilt angles or when we do not impose a restriction on dipole tilt angle. We therefore conclude that the magnetosphere only exhibits the explicit B_y effect when the dipole tilt is large, and that the general trend of more frequent onsets for $B_y > 0$ compared to $B_y < 0$ observed in the N&G list is a result on the ionospheric conditions and not the magnetospheric response.

Acknowledgments

This study was supported by the Research Council of Norway/CoE under contract 223252/F50. The OMNI solar wind data was downloaded from `https://cdaweb.gsfc.nasa.gov/sp_phys/data/omni/hro_1min/`. The AL index used in this paper was provided by the WDC for Geomagnetism, Kyoto (`http://wdc.kugi.kyoto-u.ac.jp/wdc/Sec3.html`), and downloaded as part of the OMNI data set. We gratefully acknowledge the SuperMAG collaborators (`http://supermag.jhuapl.edu/info/?page=acknowledgement`). The N&G list was downloaded from `http://supermag.jhuapl.edu/substorms/?tab=download`. The McP&C list was obtained from `https://agupubs.onlinelibrary.wiley.com/doi/full/10.1002/2017JA024766`. The Wp index, from which we derived the Nosé list, was downloaded from `http://www.isee.nagoya-u.ac.jp/~nose.masahito/s-cubed/`. The B&Y

list was obtained from `https://agupubs.onlinelibrary.wiley.com/doi/abs/10.1002/2016JA023625`. The IMAGE FUV onsets were obtained from `http://sprg.ssl.berkeley.edu/image/` and the Polar UVI onsets from `https://agupubs.onlinelibrary.wiley.com/doi/full/10.1029/2010JA015578`. We thank K. M. Laundal for providing software to calculate the dipole tilt angle (`https://github.com/klaundal/dipole`).

References

Akasofu, S.-I. (1964). The development of the auroral substorm. *Planetary and Space Science*, *12*(4), 273 - 282. doi: https://doi.org/10.1016/0032-0633(64)90151-5

Beharrell, M. J., Honary, F., Rodger, C. J., & Clilverd, M. A. (2015). Substorm-induced energetic electron precipitation: Morphology and prediction. *Journal of Geophysical Research: Space Physics*, *120*(4), 2993-3008. doi: 10.1002/2014JA020632

Borovsky, J. E., & Cayton, T. E. (2011). Entropy mapping of the outer electron radiation belt between the magnetotail and geosynchronous orbit. *Journal of Geophysical Research: Space Physics*, *116*(A6), A06216. doi: 10.1029/2011JA016470

Borovsky, J. E., & Yakymenko, K. (2017). Substorm occurrence rates, substorm recurrence times, and solar wind structure. *Journal of Geophysical Research: Space Physics*, *122*(3), 2973-2998. doi: 10.1002/2016JA023625

Boscher, D., Bourdarie, S., O'Brien, P., & Guild, T. (2004–2008). *Irbem library v4. 3.* Retrieved from `https://sourceforge.net/projects/irbem/`

Chu, X., McPherron, R. L., Hsu, T.-S., & Angelopoulos, V. (2015). Solar cycle dependence of substorm occurrence and duration: Implications for onset. *Journal of Geophysical Research: Space Physics*, *120*(4), 2808-2818. doi: 10.1002/2015JA021104

Cowley, S. W. H. (1981). Magnetospheric asymmetries associated with the Y-component of the IMF. *Planetary and Space Science*, *29*(1), 79 - 96. doi: https://doi.org/10.1016/0032-0633(81)90141-0

Dimmock, A. P., Nykyri, K., Osmane, A., & Pulkkinen, T. I. (2016). Statistical mapping of ULF Pc3 velocity fluctuations in the Earth's dayside magnetosheath as a function of solar wind conditions. *Advances in Space Research*, *58*(2), 196–207. doi: 10.1016/j.asr.2015.09.039

Fairfield, D. (1980). A statistical determination of the shape and position of the geomagnetic neutral sheet. *Journal of Geophysical Research: Space Physics*, *85*(A2), 775-780. doi: 10.1029/JA085iA02p00775

Forsyth, C., Rae, I. J., Coxon, J. C., Freeman, M. P., Jackman, C. M., Gjerloev, J., & Fazakerley, A. N. (2015). A new technique for determining Substorm Onsets and Phases from Indices of the Electrojet (SOPHIE). *Journal of Geophysical Research: Space Physics*, *120*(12), 10,592-10,606. doi: 10.1002/2015JA021343

Frey, H. U., & Mende, S. B. (2006). Substorm onsets as observed by IMAGE-FUV. In *Proceedings of the 8th international conference on substorms* (pp. 71–76).

Frey, H. U., Mende, S. B., Angelopoulos, V., & Donovan, E. F. (2004). Substorm onset observations by IMAGE-FUV. *Journal of Geophysical Research: Space Physics*, *109*(A10), A10304. doi: 10.1029/2004JA010607

Friis-Christensen, E., & Wilhjelm, J. (1975). Polar cap currents for different directions of the interplanetary magnetic field in the Y-Z plane. *Journal of Geophysical Research (1896-1977)*, *80*(10), 1248-1260. doi: 10.1029/JA080i010p01248

Gjerloev, J. W. (2012). The supermag data processing technique. *Journal of Geophysical Research: Space Physics*, *117*(A9), A09213. doi: 10.1029/2012JA017683

Grocott, A., Milan, S. E., Yeoman, T. K., Sato, N., Yukimatu, A. S., & Wild, J. A.

(2010). Superposed epoch analysis of the ionospheric convection evolution during substorms: IMF BY dependence. *Journal of Geophysical Research: Space Physics*, *115*(A5), A00106. doi: 10.1029/2010JA015728

Grocott, A., Wild, J. A., Milan, S. E., & Yeoman, T. K. (2009). Superposed epoch analysis of the ionospheric convection evolution during substorms: onset latitude dependence. *Annales Geophysicae*, *27*(2), 591–600. doi: 10.5194/angeo-27-591-2009

Holappa, L., Asikainen, T., & Mursula, K. (2020). Explicit IMF dependence in geomagnetic activity: Modulation of precipitating electrons. *Geophysical Research Letters*, *47*(4), e2019GL086676. doi: 10.1029/2019GL086676

Holappa, L., & Mursula, K. (2018). Explicit IMF By dependence in high-latitude geomagnetic activity. *Journal of Geophysical Research: Space Physics*, *123*(6), 4728-4740. doi: 10.1029/2018JA025517

Kamide, Y., & McIlwain, C. E. (1974). The onset time of magnetospheric substorms determined from ground and synchronous satellite records. *Journal of Geophysical Research (1896-1977)*, *79*(31), 4787-4790. doi: 10.1029/JA079i031p04787

King, J. H., & Papitashvili, N. E. (2005). Solar wind spatial scales in and comparisons of hourly wind and ace plasma and magnetic field data. *Journal of Geophysical Research: Space Physics*, *110*(A2), A02104. doi: 10.1029/2004JA010649

Koga, D., Gonzalez, W. D., Souza, V. M., Cardoso, F. R., Wang, C., & Liu, Z. K. (2019). Dayside Magnetopause Reconnection: Its Dependence on Solar Wind and Magnetosheath Conditions. *Journal of Geophysical Research: Space Physics*, *124*(11), 8778–8787. doi: 10.1029/2019JA026889

Laundal, K. M., Finlay, C. C., Olsen, N., & Reistad, J. P. (2018). Solar wind and seasonal influence on ionospheric currents from Swarm and CHAMP measurements. *Journal of Geophysical Research: Space Physics*, *123*(5), 4402-4429. doi: 10.1029/2018JA025387

Laundal, K. M., & Richmond, A. D. (2017). Magnetic coordinate systems. *Space Science Reviews*, *206*, 27-59. doi: 10.1007/s11214-016-0275-y

Liou, K. (2010). Polar Ultraviolet Imager observation of auroral breakup. *Journal of Geophysical Research: Space Physics*, *115*(A12), A12219. doi: 10.1029/2010JA015578

Liou, K., & Newell, P. T. (2010). On the azimuthal location of auroral breakup: Hemispheric asymmetry. *Geophysical Research Letters*, *37*(23), L23103. doi: 10.1029/2010GL045537

Liou, K., Sotirelis, T., & Mitchell, E. (2020). Control of the east-west component of the interplanetary magnetic field on the occurrence of magnetic substorms. *Geophysical Research Letters*, *47*(5), e2020GL087406. doi: 10.1029/2020GL087406

McPherron, R. L., & Chu, X. (2018). The midlatitude positive bay index and the statistics of substorm occurrence. *Journal of Geophysical Research: Space Physics*, *123*(4), 2831-2850. doi: 10.1002/2017JA024766

Milan, S. E., Gosling, J. S., & Hubert, B. (2012). Relationship between interplanetary parameters and the magnetopause reconnection rate quantified from observations of the expanding polar cap. *Journal of Geophysical Research: Space Physics*, *117*(A3), A03226. doi: 10.1029/2011JA017082

Milan, S. E., Walach, M.-T., Carter, J. A., Sangha, H., & Anderson, B. J. (2019). Substorm onset latitude and the steadiness of magnetospheric convection. *Journal of Geophysical Research: Space Physics*, *124*(3), 1738-1752. doi: 10.1029/2018JA025969

Morley, S. K., Koller, J., Welling, D. T., Larsen, B. A., Henderson, M. G., & Niehof, J. T. (2011). Spacepy - A Python-based library of tools for the space sciences. In *Proceedings of the 9th Python in science conference (SciPy 2010).* Austin,

TX.
Newell, P. T., & Gjerloev, J. W. (2011a). Evaluation of SuperMAG auroral electrojet indices as indicators of substorms and auroral power. *Journal of Geophysical Research: Space Physics*, *116*(A12), A12211. doi: 10.1029/2011JA016779

Newell, P. T., & Gjerloev, J. W. (2011b). Substorm and magnetosphere characteristic scales inferred from the SuperMAG auroral electrojet indices. *Journal of Geophysical Research: Space Physics*, *116*(A12), A12232. doi: 10.1029/2011JA016936

Newell, P. T., Liou, K., Gjerloev, J. W., Sotirelis, T., Wing, S., & Mitchell, E. J. (2016). Substorm probabilities are best predicted from solar wind speed. *Journal of Atmospheric and Solar-Terrestrial Physics*, *146*, 28 - 37. doi: https://doi.org/10.1016/j.jastp.2016.04.019

Nosé, M., Iyemori, T., Wang, L., Hitchman, A., Matzka, J., Feller, M., … Çelik, C. (2012). Wp index: A new substorm index derived from high-resolution geomagnetic field data at low latitude. *Space Weather*, *10*(8), S08002. doi: 10.1029/2012SW000785

Nykyri, K., Ma, X., Dimmock, A., Foullon, C., Otto, A., & Osmane, A. (2017). Influence of velocity fluctuations on the Kelvin-Helmholtz instability and its associated mass transport. *Journal of Geophysical Research: Space Physics*, *122*(9), 9489–9512. doi: 10.1002/2017JA024374

Paschmann, G., Papamastorakis, I., Baumjohann, W., Sckopke, N., Carlson, C. W., Sonnerup, B. U. Ö., & Lühr, H. (1986). The magnetopause for large magnetic shear: AMPTE/IRM observations. *Journal of Geophysical Research*, *91*(A10), 11099. doi: 10.1029/ja091ia10p11099

Reistad, J. P., Laundal, K. M., Ohma, A., Moretto, T., & Milan, S. E. (2020). An explicit IMF b_y dependence on solar wind-magnetosphere coupling. *Geophysical Research Letters*, *47*(1), e2019GL086062. doi: 10.1029/2019GL086062

Russell, C. T., & Brody, K. I. (1967). Some remarks on the position and shape of the neutral sheet. *Journal of Geophysical Research (1896-1977)*, *72*(23), 6104-6106. doi: 10.1029/JZ072i023p06104

Russell, C. T., & McPherron, R. L. (1973). Semiannual variation of geomagnetic activity. *Journal of Geophysical Research (1896-1977)*, *78*(1), 92-108. doi: 10.1029/JA078i001p00092

Sergeev, V. A., Pellinen, R. J., & Pulkkinen, T. I. (1996). Steady magnetospheric convection: A review of recent results. *Space Science Reviews*, *75*(3-4), 551–604.

Tsyganenko, N. A., & Fairfield, D. H. (2004). Global shape of the magnetotail current sheet as derived from Geotail and Polar data. *Journal of Geophysical Research: Space Physics*, *109*(A3), A03218. doi: 10.1029/2003JA010062

Walsh, A. P., Haaland, S., Forsyth, C., Keesee, A. M., Kissinger, J., Li, K., … Taylor, M. G. (2014). Dawn-dusk asymmetries in the coupled solar wind-magnetosphere-ionosphere system: A review. *Annales Geophysicae*, *32*(7), 705–737. doi: 10.5194/angeo-32-705-2014

Weygand, J. M., McPherron, R., Kauristie, K., Frey, H., & Hsu, T.-S. (2008). Relation of auroral substorm onset to local al index and dispersionless particle injections. *Journal of Atmospheric and Solar-Terrestrial Physics*, *70*(18), 2336 - 2345. doi: https://doi.org/10.1016/j.jastp.2008.09.030

Yeoman, T. K., Freeman, M. P., Reeves, G. D., Lester, M., & Orr, D. (1994). A comparison of midlatitude Pi 2 pulsations and geostationary orbit particle injections as substorm indicators. *Journal of Geophysical Research: Space Physics*, *99*(A3), 4085-4093. doi: 10.1029/93JA03233